frontiers in Energy Research

ORIGINAL RESEARCH
published: 17 September 2021
doi: 10.3389/fenrg.2021.746109

In Situ Hydrodeoxygenation of Lignin-Derived Phenols With Synergistic Effect Between the Bimetal and Nb_2O_5 Support

Le Tong[1,2], *Bo Cai*[1,2], *Ronghua Zhang*[1], *Junfeng Feng*[1,2,3]* *and Hui Pan*[1,2]*

[1]*Jiangsu Co-Innovation Centre of Efficient Processing and Utilization of Forest Resources, Jiangsu Provincial Key Lab for the Chemistry and Utilization of Agro-Forest Biomass, College of Chemical Engineering, Nanjing Forestry University, Nanjing, China,* [2]*International Innovation Center for Forest Chemicals and Materials, Nanjing Forestry University, Nanjing, China,* [3]*Jiangsu Key Laboratory for Biomass Energy and Material Institute of Chemical Industry of Forest Products, Chinese Academy of Forestry, National Engineering Lab. for Biomass Chemical Utilization, Jiangsu Key Laboratory for Biomass Energy and Material, Nanjing, China*

OPEN ACCESS

Edited by:
Xiaojun Shen,
Dalian National Laboratory for Clean Energy, Dalian Institute of Chemical Physics (CAS), China

Reviewed by:
Riyang Shu,
Guangdong University of Technology, China
Yaxuan Jing,
East China University of Science and Technology, China
Yu Xin,
Institute of Chemistry (CAS), China

***Correspondence:**
Junfeng Feng
2018149@njfu.edu.cn
Hui Pan
hpan@njfu.edu.cn

Specialty section:
This article was submitted to Bioenergy and Biofuels, a section of the journal Frontiers in Energy Research

Received: *23 July 2021*
Accepted: *18 August 2021*
Published: *17 September 2021*

Citation:
Tong L, Cai B, Zhang R, Feng J and Pan H (2021) In Situ *Hydrodeoxygenation of Lignin-Derived Phenols With Synergistic Effect Between the Bimetal and Nb_2O_5 Support. Front. Energy Res. 9:746109. doi: 10.3389/fenrg.2021.746109*

Nb_2O_5-supported bimetallic catalysts were prepared by the impregnation method applied for the *in situ* hydrogenation of guaiacol. Guaiacol can be effectively transformed into cyclohexanol over different bimetallic catalysts using alcohol as the hydrogen donor. Meanwhile, the effects of different hydrogen donors such as isopropanol, sec-pentanol, and ethylene glycol on *in situ* hydrogenation of guaiacol were investigated in detail, and the results showed that isopropanol is the best hydrogen supply solvent. Then, the dependence of Ni–Mn/Nb_2O_5 properties on metal loading, reaction time, reaction temperature, and reaction pressure was studied for the *in situ* hydrogenation of guaiacol by using isopropanol as the hydrogen donor. Guaiacol can be completely converted, and the yield of cyclohexanol reached 71.8% over Ni–Mn/Nb_2O_5 with isopropanol as the hydrogen donor at 200°C for 5 h. The structures and characteristics of better catalytic properties of the Ni–Mn/Nb_2O_5 catalyst were determined by BET, NH_3-TPD, XRD, XPS, SEM, and TEM, and the results indicated the particle size of the metal was small (approximately 10 nm) and the metal particles are finely dispersed in the whole support. Therefore, a large number of medium acid sites were generated on the 10Ni-10Mn/Nb_2O_5 with a large specific surface area, which could increase the interface between the metal and the support and may be beneficial to the hydrodeoxygenation of guaiacol.

Keywords: *in situ* hydrodeoxygenation, phenol compounds, bimetallic and bifunctional catalyst, cyclohexanol, Nb_2O_5

INTRODUCTION

Lignocellulosic biomass is the largest renewable resource in nature and an ideal substitute for fossil energy (Mushtaq et al., 2015). It can be converted into transportation fuel (bio-oil) or fine chemicals and can also overcome the environmental challenges in using fossil energy. However, due to the complex components of bio-oil, there are shortcomings such as thermal instability, low calorific value, and high viscosity and cannot be widely used. These shortcomings are mainly caused by the large number of oxygen-containing compounds contained in the bio-oil, including aldehydes, acids,

and phenol. Among them, phenolic compounds derived from lignin (Ragauskas et al., 2014) are the main components of bio-oil. Therefore, to expand the wide application of bio-oil, it needs to be upgraded by reducing the oxygen content.

At present, the more commonly used methods for upgrading and refining bio-oil or lignin degradation products in domestic and foreign research include catalytic reforming, catalytic cracking, and catalytic hydrodeoxygenation. Catalytic hydrodeoxygenation (HDO) is one of the more important ones. Under the action of a specific catalyst, the bio-oil can be catalytically hydrogenated by pressurized external hydrogen supply or hydrogen generated by solvent (*in situ* hydrogenation), and the phenolic compounds in the bio-oil are refined into liquid fuels such as alkanes. The HDO operation of bio-oil can remove the oxygen in bio-oil by water or alcohol, increase the effective hydrogen–carbon ratio, reduce oxygen content, and improve the quality of bio-oil.

In previous studies, many catalysts applied to the hydrodeoxygenation process with excellent performance have been reported. Among them, precious metals [Pt (Zhu et al., 2011; Saidi et al., 2014; He et al., 2018; Funkenbusch et al., 2019), Pd (Rahzani et al., 2017), Rh (Wang et al., 2008; Chen et al., 2016), Au (Ferentz et al., 2015; Qin et al., 2019), Ag (Liu et al., 2019), Ru (Newman et al., 2014; Ma et al., 2019)] have attracted much attention in the HDO research of phenolic compounds because of their remarkable catalytic hydrogenolysis and catalytic hydrogenation capabilities. For example, Funkenbusch et al. (2019) studied the catalytic performance of Pt/Al_2O_3 using phenolic model compounds (anisole, phenol, and m-cresol) as reactants. And, the results showed that the Pt/Al_2O_3 catalyst exhibited good ring saturation, demethylation, and enhanced deoxygenation. Wang et al. (2008) prepared the Rh/CNF catalyst with an average particle size of 2-3 nm, and the metal was highly dispersed on the CNF support by using the incipient wetness impregnation method. The results of the Rh/CNF catalyst applied in the hydrogenation reaction of phenols suggested that the aromatic ring in phenols was hydrogenated and the yield of the target product cyclohexanone could reach 60%. Chen et al. (2015) used the impregnation method to prepare a supported Ru/CNT catalyst and then used for the deoxygenation of phenolic compounds. Under the conditions of a reaction temperature of 220°C and a hydrogen pressure of 5 MPa, the conversion of eugenol can reach 100% with Ru/CNT and the selectivity of HDO product (4-propylcyclohexane) was as high as 94%. Under mild conditions, noble metal catalysts have excellent adsorption capacity for reactants and active hydrogen generated in the hydrogenation process, so they have better catalytic performance and high activity for deoxygenated products than other catalysts. However, noble metal catalysts are too expensive and prone to inactivate (Ohta et al., 2014). The upgrading of bio-oils with large-scale production using noble metal catalysts requires high economic costs, thus limiting their commercial applications. Nonprecious metal catalysts are more cost-effective than precious metal catalysts and show acceptable catalytic performance in HDO of phenolic compounds. Among these nonprecious metal catalysts (Co (Han et al., 2019), Mo (Yang et al., 2019), Ni, etc.), nickel-based (Qiu et al., 2016; Zhang et al., 2018; Lu et al., 2019; Resende et al., 2019; Li et al., 2020; Shafaghat et al., 2020; Song et al., 2020) catalysts have been extensively studied for the hydrodeoxygenation of different bio-oil model compounds. Therefore, nonprecious metal catalysts represented by nickel-based catalysts have attracted much attention because of their high hydrogenation activity and low cost. It can effectively convert hydrogen into active hydrogen and then apply it to the hydrogenation of phenolic compounds. It exhibits high hydrogenation activity in the hydrogenation process of phenolic compounds with good stability. Loading nickel metal on a carrier (metal oxides, molecular sieves, carbon materials, etc.) with special functions can better exert the catalytic hydrogenation effect of nickel metal (Mortensen et al., 2016; Bjelić et al., 2019; Li et al., 2020). And, in supported catalysts, the support materials are also a key factor in determining catalytic performance, as the metal is the hydrogenation active center and the carrier provides acid sites for the HDO reaction. Metal oxides (Al_2O_3 (Zhao et al., 2011), SiO_2 (Li et al., 2015), TiO_2 (Shu et al., 2019), Nb_2O_5 (Kon et al., 2014; Jin et al., 2017; Song et al., 2020), etc.) are selected as catalyst supports due to their excellent performance. For example, Al_2O_3 was widely used as a catalyst carrier for HDO catalysts due to its low price, excellent texture, and moderate acidity. Besides, SiO_2 was also used as a catalyst support due to its large specific surface area. In the study of hydrodeoxygenation of bio-oil phenolic compounds, the kinds of main products and the selectivity of the product varied with different catalysts with distinguishing metals and carriers. Furthermore, bimetallic catalysts offered the possibility of improving catalyst performance and adjusting the selectivity of specific products compared with monometallic catalysts. In the bimetallic catalyst, the interaction between the bimetal and the support can improve the catalytic activity of the catalyst, which is beneficial to promote the HDO reaction of phenolic compounds. For example, Ohta et al. (2014) selected ZrO_2 as the carrier and prepared a Pt–Re/ZrO_2 catalyst by the impregnation method. Under the reaction conditions of 300°C and 2 MPa hydrogen, the catalytic performance was studied in the HDO reaction of the lignin model compound 4-propylphenol. The results show that compared with Pt/ZrO_2, the incorporation of Re metal in Re/ZrO_2 or Re–Pt/ZrO_2 is beneficial to improve the catalyst stability and can increase the yield and selectivity of the deoxygenated product. The reaction path followed the benzene ring hydrogenation-dehydration-dehydrogenation step in 4-propylphenol converting to 4-propylbenzene. Moreover, the selectivity of target products such as propyl benzene is as high as 80%, and Re metal can inhibit Pt from sintering at high temperature (300°C), which is beneficial to prevent and control catalyst deactivation. In general, the advantage of the bimetallic catalyst is that the interaction between the two metals can significantly improve the catalytic performance of the catalyst, which is beneficial to adjust the selectivity of the final product. In addition, the adjustment effect of the auxiliary metal on the oxygenphilic active site and the ability to improve the dispersion of the active phase are also the main advantages of the bimetallic catalyst.

On the other hand, many hydrogenation experiments of bio-oil or phenolic model compounds used the external hydrogen

sources. However, the traditional hydrogenation process conditions using external hydrogen are more difficult and will harm the reactor and the catalyst (causing reactor blockage and catalyst deactivation) (Shafaghat et al., 2020), limiting its industrial application. Therefore, some studies are devoted to finding a way to replace external hydrogen supply, which could produce the same hydrogen supply effect at relatively mild operating conditions. Among them, *in situ* hydrogenation is a very effective alternative method. *In situ* hydrogenation uses hydrogen-donating solvents such as lower alcohols to undergo reforming reaction with water to generate active hydrogen or hydrogen radicals, which can effectively provide a hydrogen source in the hydrodeoxygenation reactions of phenolic compounds. At present, there are many studies on *in situ* hydrogenation (Reddy Kannapu et al., 2015; Xu et al., 2015; Feng et al., 2017; Xu et al., 2017; Montañez Valencia et al., 2020; Shafaghat et al., 2020) of different model compounds of bio-oil. For instance, Shafaghat et al. (2020) reported that saturated cyclic compounds (cyclohexanol and cyclohexane) were produced in the *in situ* hydrogenation of phenol on Ni/CeO_2 (using 2-propanol and 2-butanol as hydrogen sources). Feng et al. (2017) used Raney nickel as a catalyst and methanol as a hydrogen donor to produce the cyclohexane and cyclohexanol derivatives in the hydrodeoxygenation reaction of guaiacol.

Because NbOx species had a strong ability to activate C-O bonds, niobium-based materials were often used as carriers in HOD. So, we choose niobium oxide as the carrier of the catalyst (Song et al., 2020). Therefore, this study prepared a series of bimetallic catalysts ($Ni–Mn/Nb_2O_5$, $Ni–Zr/Nb_2O_5$, $Ni–Cu/Nb_2O_5$, $Ni–Mo/Nb_2O_5$, and $Ni–Co/Nb_2O_5$) with Nb_2O_5 as the support and studied the hydrogenation process of lignin-derivative phenolic compounds by using a low-carbon alcohol and water composite solvent to *in situ* produce active hydrogen. The prepared Ni and Mn bimetallic catalysts supported on niobium oxide and isopropanol/water hydrogen supply system can efficiently convert guaiacol into cyclohexanol. By analyzing the structural characteristics of the catalyst, it is found that the better catalytic performance of the $Ni–Mn/Nb_2O_5$ catalyst is due to the structural characteristics of large pores and larger specific surface area. The catalyst can completely convert the lignin-derived phenolic compounds into cyclohexanol, cyclohexane, etc., and the selectivity and yield of the main product cyclohexanol were outstanding.

EXPERIMENTAL

Reagents and Materials

All reagents and solvents were of analytical grade, provided by commercial suppliers and used without further purification, unless otherwise noted. High-purity commercial niobium oxide was purchased from Aladdin Chemical Reagent. $Ni(NO_3)_2$ $6H_2O$ was purchased from Nanjing Chemical Reagent Co., Ltd. $Mn(CH_3COO)_2$ $4H_2O$ was purchased from Xilong Chemical Co., Ltd.

Catalyst Synthesis

A typical synthesis of bimetallic catalyst (Ni–Co/Cu/Mo/Zr/Mn) was the incipient wetness impregnation method. A certain amount of Nb_2O_5 and metal precursor were dispersed in deionized water (DI) for 1 h by ultrasonic and then magnetically stirred for 4 h to promote metal adsorption on the support. Subsequently, the solution was vacuum-dried using a rotary evaporator to a viscous state and further dried overnight at 120°C in an oven. After that, the prepared catalysts were finally calcinated in air at 500°C for 5 h with a heating rate of 5°C/min, then ground with a mortar and pestle, and reduced in 20 vol% H_2 in N_2 gas at 500°C for 5 h. The heating rate was 5°C/min.

Catalyst Characterization

The specific surface area, pore volume, and pore diameter of the catalyst sample are measured by the N_2 adsorption–desorption method at liquid nitrogen temperature at −196°C on a bedside instrument (3H-2000PS1). All data from the surface of the catalyst are calculated and determined by using Brunauer–Emmett–Teller (BET) equation and *t*-plot obtained from the isotherms. X-ray diffraction analysis (XRD) was implemented on the Ultima IV instrument equipped with Cu Kα radiation to observe the phase composition of the catalyst sample. The powder XRD spectrum test range of the catalyst sample is from 5° to 80° with a scan rate of 1°/min. Scanning electron microscope (SEM) measurement was performed on the Phenom LE instrument with an accelerating voltage of 15 kV to observe the surface morphology of the catalyst, and energy dispersive spectrometry (EDS) was carried out on a coupled AZtec, Oxford, to determine the elemental composition and weight proportion of metal on the surface of catalysts. The transmission electron microscope (TEM) measurement was carried out on the Jeol JEM 2100 F instrument with an accelerating voltage of 200 kV. XPS measurement was performed on the AXIS UltraDLD instrument equipped with an Al Ka X-ray anode source to determine the chemical state of the elements on the catalyst. The peaks of the XPS spectrum were corrected by the binding energy of C 1s (284.6 eV). NH_3-TPD by a Mike AutoChem II 2920 was implemented to measure the acidity of the catalyst. Using NH_3 as the probe molecule, the sample to be characterized is quantitatively adsorbed at room temperature, and then N_2 is used as the desorption medium to desorb NH_3 adsorbed on the sample under temperature-programmed conditions. Before TPD analysis, the sample was first reduced at 400°C for 60 min in Ar airflow with a gas flow velocity of 30 ml min^{-1}. Then, it was cooled to 100°C under Ar flow and exposed to 10% NH_3/90% Ar logistics of 30 ml min^{-1} at this temperature for 30 min. Finally, the sample was rinsed with Ar (90 min) to eliminate the physically adsorbed NH_3. Ammonia desorption was measured by increasing the sample temperature to 800°C (10°C min^{-1}) under Ar airflow (30 ml min^{-1}).

Catalyst Testing

The catalytic activity test was carried out in a 50 ml stainless steel autoclave equipped with magnetic stirring. The catalyst (0.5 g), solvent water (20 g), isopropanol (5 g), and guaiacol (1 g) were charged into the autoclave for each run. 1 MPa of nitrogen is

flushed to heat the reactor to the desired reaction temperature while stirring at 800 rpm. After the reaction was completed, the reaction kettle was cooled down to room temperature in air, and the liquid was collected for subsequent analysis. The solvent after the reaction was extracted with ethyl acetate to separate the organic phase. The organic phase was qualitatively analyzed using a gas chromatograph equipped with an HP-5 column and FID detector. Naphthalene was used as an internal standard for quantitative analysis of liquid products. The conversion of the reactants and the product composition and yield were defined by GC and GC-MS.

The conversion of the products and the yield of the products were calculated based on the following formula. For the repeatability test experiment of the catalyst, the used catalyst was separated by suction filtration, washed with water and ethanol for more than three times, dried at 105°C for 12 h, and then reused. Due to the partial weight loss of the catalyst during the operation, fresh unused catalyst was added to compensate before the next reaction.

$$\text{Conv.}\,(\text{mol\%}) = \frac{\textit{moles of substrate changed into product}}{\textit{initial moles of the substrate}} \times 100\%, \quad (1)$$

$$\text{product yield}\,(\text{mol\%}) = \frac{\textit{moles of product}\,(A)}{\textit{moles of the reacted substrate}} \times 100\%. \quad (2)$$

Product Analysis

By gas chromatography (Shimadzu GC-2010 with FID detector and DB-5 column) and GC-MS (Agilent 7890A-5975C with DB-FFAP capillary column), the liquid products obtained from the HDO of phenolic compounds were analyzed. The oven temperature program was increased from 50°C (hold for 1 min) to 260°C (hold for 10 min) at a rate of 10°C/min.

RESULTS AND DISCUSSION

As one of the most representative phenolic monomers derived from lignin, guaiacol containing phenolic hydroxyl and methoxy groups was selected as the phenolic model. During the *in situ* hydrogenation of guaiacol, the target product was cyclohexanol. The initial experiments were carried out to investigate the catalyst activities towards the HDO of guaiacol used in isopropanol/water as hydrogen supply solvent. Herein, the hydrodeoxygenation of guaiacol was carried out over 15Ni/Nb_2O_5 and Ni-based bimetallic catalyst with Nb_2O_5 as support. The conversion of guaiacol and yield of the target product cyclohexanol with various nickel-based bimetallic catalysts is presented in **Supplementary Table S1**. It could be clearly found that both the conversion of guaiacol and molar yield of main product were greatly affected by the change of active metal composition in catalyst. These results indicated that not all selected bimetals could promote the deoxygenation reaction of guaiacol. It was clearly shown that cyclohexanol was the main product in all nickel-based bimetallic catalysts under the same conditions. The addition of the second metal had a significant effect on the conversion of guaiacol. Initially, in entry 1–5, diversified nickel-based bimetallic catalysts were used to investigate the HDO of guaiacol in water/isopropanol-mixed solvents under the reaction conditions of reaction temperature 220°C kept for 5 h. As the results shown, all 15Ni-15Mn/Nb_2O_5, 15Ni-15Zr/Nb_2O_5, and 15Ni-15Co/Nb_2O_5 exhibited good catalytic performance in the HDO of guaiacol, the conversion was 100, 100, and 61.9%, respectively, and the yields of the main product cyclohexanol were 76.2 mol%, 61 mol%, and 60 mol%, respectively. However, 15Ni-15Cu/Nb_2O_5 and 15Ni-15Mo/Nb_2O_5 showed lower catalyst activity with the guaiacol conversion being 29 and 19%, and almost no target product cyclohexanol was detected in the product. Thus, it could be found that the addition of Cu or Mo to Ni suppressed the hydrogenation of guaiacol (entry 2 and 4).

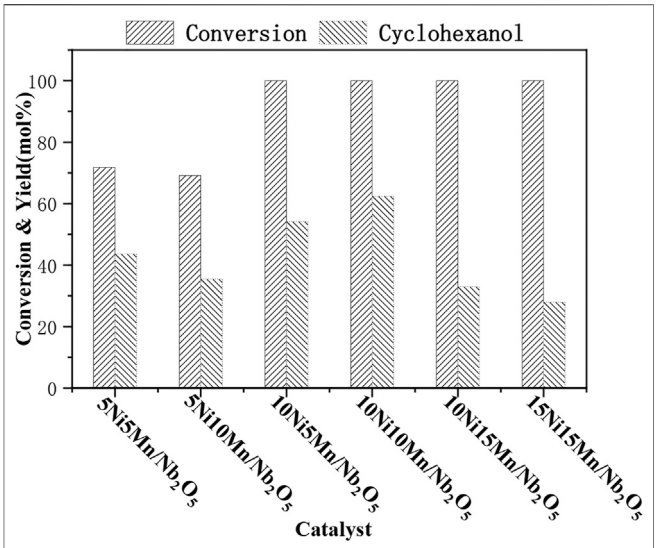

FIGURE 1 | Effect of ratio of metal loads on GUA conversion and the main product yield. Reaction conditions: 1 g GUA, 0.5 of Ni–Mn/Nb_2O_5, 1 MPa N_2, 200°C, 5 h, 5 g of isopropanol, and 20 g of water.

In addition, considering the influence of reaction conditions on the change of GUA selectivity to HDO, we tried to increase the temperature and reduce the relative content of the catalyst (reactant:catalyst = 2:1) to test the catalytic performance of these bimetallic catalysts (entry 6–10). The results shown that even though the 15Ni-15Mn/Nb_2O_5 catalyst still had good catalytic performance in the HDO of guaiacol, the yield of the main product cyclohexanol was significantly reduced, from 76.2 mol% (entry 3) to 53.32 mol% (entry 7). The same situation also appeared in 15Ni-15Zr/Nb_2O_5, and the yield of cyclohexanol decreased from 61 mol% (entry 1) to 24.4 mol% (entry 10). We speculated that this may be due to the relative reduction in the number of catalysts that caused the relative reduction of active sites, which reduced the hydrodeoxygenation efficiency of guaiacol. Besides, the increase in temperature would cause partial deactivation of the catalyst, which would reduce the catalytic performance of the catalyst.

TABLE 1 | Physicochemical structure properties of Nb_2O_5 and 10Ni-10Mn/Nb_2O_5 catalysts.

Catalyst	Surface area (m^2/g)	Micropore volume (m^3/g)	Total pore volume (cm^3/g)	Average pore size (nm)
Nb_2O_5	18.63	0.001	0.019	1.7
10Ni-10Mn/Nb_2O_5	42.77	0.003	0.056	1.9

Studies had pointed out that a short time of hydrogenation treatment led to repolymerization of the reactants in the hydrogenation process. In contrast, a longer reaction time can effectively promote the hydrogenation of the reactants (Li et al., 2014). Therefore, we tried to extend the reaction time to study the catalytic performance of the bimetallic catalyst (entry 11–15). The results showed that the conversion of guaiacol did not change much with the increase of reaction time. However, the yield of cyclohexanol increased slightly. Compared with 15Ni-15Cu/Nb_2O_5 and 15Ni-15Mo/Nb_2O_5 without catalytic activity, 15Ni-15Mn/Nb_2O_5, 15Ni-15Zr/Nb_2O_5, and 15Ni-15Co/Nb_2O_5 exhibited good catalytic performance in the HDO of guaiacol, and the yield of main product cyclohexanol was increased to 63.6 mol%, 57.8 mol%, and 61.2 mol%, respectively. In summary, the Ni–Mn/Nb_2O_5 catalyst exhibited better catalytic activity of guaiacol HDO. Therefore, we initially selected Ni–Mn/Nb_2O_5 as the research object.

It was reported that higher metal loading amount and better dispersity would lead to the improved catalytic activity (Zhou et al., 2017a). **Figure 1** showed a marked role played by the bimetal amount (5:5, 5:10, 10:5, 10:10, 10:15, and 15:15) of the catalyst's performance. It could be clearly seen from the results that the different proportions of the two metals could significantly affect the conversion process of guaiacol and the yield of the target product in the bimetallic catalyst. When the nickel loading 10% (10Ni-10Mn/Nb_2O_5), guaiacol could be completely converted, and the yield of cyclohexanol was highest (72 mol%).

When the nickel metal loading was 5 and 10%, the activity of the bimetallic catalyst increases with the increase of the loading, and the yield of the target product also increases from 35.5 mol% to 62.5 mol%. When the loading of nickel and manganese was both 10%, the conversion rate of guaiacol and the yield of cyclohexanol both reached the highest. At the same time, when the Ni metal loading was above 10%, the conversion rate of guaiacol could reach 100%, indicating that Ni metal contributed to the conversion of guaiacol. However, when the loading of Mn metal increased to 15% (10Ni-15Mn/Nb_2O_5 and 15Ni-15Mn/Nb_2O_5), the activity of the catalyst decreased, and the yield of the target product and the conversion rate of guaiacol was both decreased. We speculated that this may be due to (1) a part of the nickel metal phase may be covered by the manganese support; (2) when too much metal was loaded into Nb_2O_5, it would change the surface and pore distribution of the catalyst and then affect the hydrogenation activity of the catalyst. Finally, comprehensive research on the performance of guaiacol HDO with all different metal loading catalysts was carried out and selected 10Ni-10Mn/Nb_2O_5 catalyst as the research object. Following, we analyzed the specific structure of the catalyst to further analyze the reason.

Catalyst Characterization

Table 1 summarizes the textural properties of the Nb_2O_5 support and 10Ni-10Mn/Nb_2O_5. The specific surface area of Nb_2O_5 used in this work determined through the BET is 18.63 $m^2\ g^{-1}$. Compared with the Nb_2O_5 support, the Ni-based bimetallic catalyst 10Ni-10Mn/Nb_2O_5 exhibited a higher specific surface area of 42.77 $m^2\ g^{-1}$. The increasing of specific surface area may be due to the intrusion of metal playing a role in expanding the pores of the support. Moreover, the microspore volume and pore size of 10Ni-10Mn/Nb_2O_5 catalyst was better than the Nb_2O_5 support, which means the presence of metals could change structure and produce more pores of Nb_2O_5 during the preparation process. The 10Ni-10Mn/Nb_2O_5 catalyst displayed a better specific surface area and larger pore size, which may be beneficial to the hydrodeoxygenation of guaiacol.

The morphological features of the fresh catalyst were studied by scanning electron microscopy (SEM), while the chemical composition of the catalyst and the weight proportion of metal were proved by elemental spectra of the catalyst with energy dispersive X-ray analysis (EDS). The SEM images of the Nb_2O_5 support and 10Ni-10Mn/Nb_2O_5 catalyst are presented in **Figures 2A,B**. As shown above, the shape of the Nb_2O_5 support was relatively neat, whereas a small amount of particle aggregation and accumulation had occurred. Besides, the composition (wt% and at%) of the elements Ni and Mn in 10Ni-10Mn/Nb_2O_5 catalyst is summarized in the table near **Figure 2C**. EDS showed that the weight ratio of Ni to Mn on the catalyst surface of 10Ni-10Mn/Nb_2O_5 was 1.02:0.98, which was close to the theoretical loading ratio of Ni to Mn (1:1) for catalyst. It clearly shown that the Ni and Mn metal particles were well impregnated on the surface of the Nb_2O_5 support. It should be noted that the surface of the Nb_2O_5 support was smooth and flat in **Figure 2A**, and it was difficult to observe the metal particles on the surface of 10Ni-10Mn/Nb_2O_5 catalyst in **Figure 2B**. However, EDS chemical component analysis could confirm that the metal particles were finely dispersed in the whole support, which were agreed with the result of the XRD spectrum analysis of catalyst.

The TEM images are shown in **Figure 3**, the image of the Nb_2O_5 support is shown in **Figures 3A,B**, and the image of the 10Ni-10Mn/Nb_2O_5 is displayed in **Figures 3C,D**. As can be seen from **Figure 3A**, light and dark images appear on the surface of the support because the particle size of the support was too large for electrons to penetrate completely. There was no obvious particle agglomeration on the surface of Nb_2O_5 support in **Figure 3C**, which indicated that the Ni and Mn metal nanoparticles were well dispersed in the whole detection area. **Figure 3B** shows that the lattice fringe spacing of the Nb_2O_5 was 0.44 nm. The fringe distances (0.44 and 0.27 nm) shown in **Figure 3D** were consistent with the (001) and (111) planes of

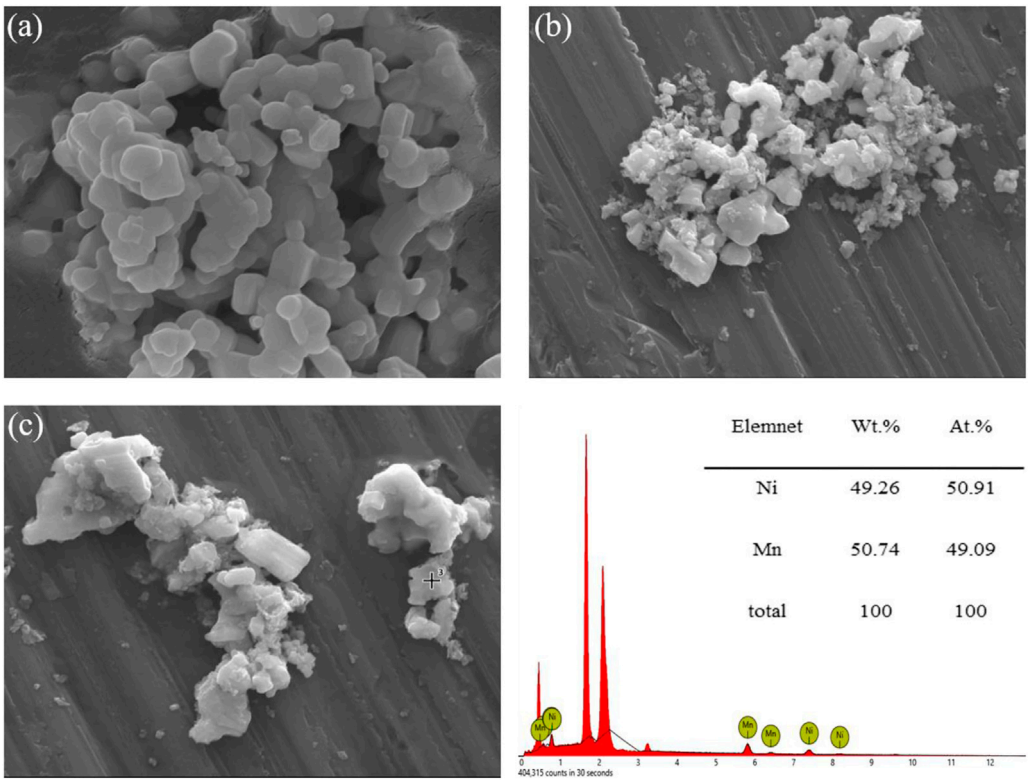

FIGURE 2 | SEM images of **(A)** 20000x Nb_2O_5, **(B)** 20000x and **(C)** 30000x 10Ni-10Mn/Nb_2O_5 samples.

Nb_2O_5 and metallic Ni, respectively. In addition, the microstructure information of MnO_2 was not observed in the TEM image, which may be due to the smaller particle size of MnO_2. Meanwhile, the particle size of metal was small and approximately 10 nm. This result was consistent with the analysis results of XRD and SEM.

Acidity was an important factor for the hydrodeoxygenation of phenolic compounds by affecting the dehydration process of the intermediate product cyclohexanol in the hydrogenated process. NH_3-TPD was an effective method to determine the acidity of catalyst through the difference of desorption temperature, in which the desorption temperature determines the acidity distribution. According to the difference of desorption temperature, acidity could be divided into the following three types: weak acid, medium strong acid, and strong acid. In order to conduct quantitative analysis on the acidity of the catalyst, standard NH_3-TPD analysis was carried out to measure the surface acidity of Nb_2O_5 and 10Ni-10Mn/Nb_2O_5 catalyst. The area of the desorption peak represented the strength of the catalyst acidity. In general, the desorption peak below 200°C corresponds to the weak acid position, the temperature range between 200 and 350°C relates to the moderate strong acid position, and the temperature above 350°C corresponds to the strong acid position. As a result, the results of NH_3-TPD are shown in **Supplementary Figure S1**. In Nb_2O_5 support, the desorption peak was observed at 366.5°C, which was ascribed to strong acid sites. In the 10Ni-10Mn/Nb_2O_5 catalyst, two desorption peaks appeared at 295.2 and 493.7°C corresponding to medium and strong acid sites, respectively. Moreover, the acid amounts of Nb_2O_5 and 10Ni-10Mn/Nb_2O_5 are summarized in **Table 2**, and the total acid sites of Nb_2O_5 and 10Ni-10Mn/Nb_2O_5 were measured to be 0.811 and 1.854 mmolNH_3/g-cat, respectively. It was worth noting that the introduction of metal species led to the increasing of acid strength and amount. In the process of preparing the catalyst, the metal was impregnated into the pores of the Nb_2O_5 support. As a result, the 10Ni-10Mn/Nb_2O_5 catalyst contained a larger specific surface area (this result was also consistent with the result of **Table 1**). Therefore, a large number of medium acid sites could be generated with 10Ni-10Mn/Nb_2O_5 having a relatively large specific surface area and good dispersibility, which could increase the interface between the metal and the support.

The X-ray powder diffraction (XRD) spectrum of the Nb_2O_5 support and metal-loading support catalyst 10Ni-10Mn/Nb_2O_5 is presented in **Figure 4**. Compared with Nb_2O_5, it could be clearly seen that 10Ni-10Mn/Nb_2O_5 had several new diffraction peaks (detected at 52.1° and 60.9°). The diffraction peaks located at 52.1° and 60.9° were ascribed to the reflections of metallic Ni. This showed that the reduction process during the preparation of the catalyst could convert the high valence state of Ni into metallic Ni. Meanwhile, the peaks of 35.2° and 38.8° belong to the reflections of MnO_2, which suggested that the high-valence Mn was not completely reduced to metallic Mn during the preparation of the catalyst. A sharp diffraction peak with higher peak intensity was

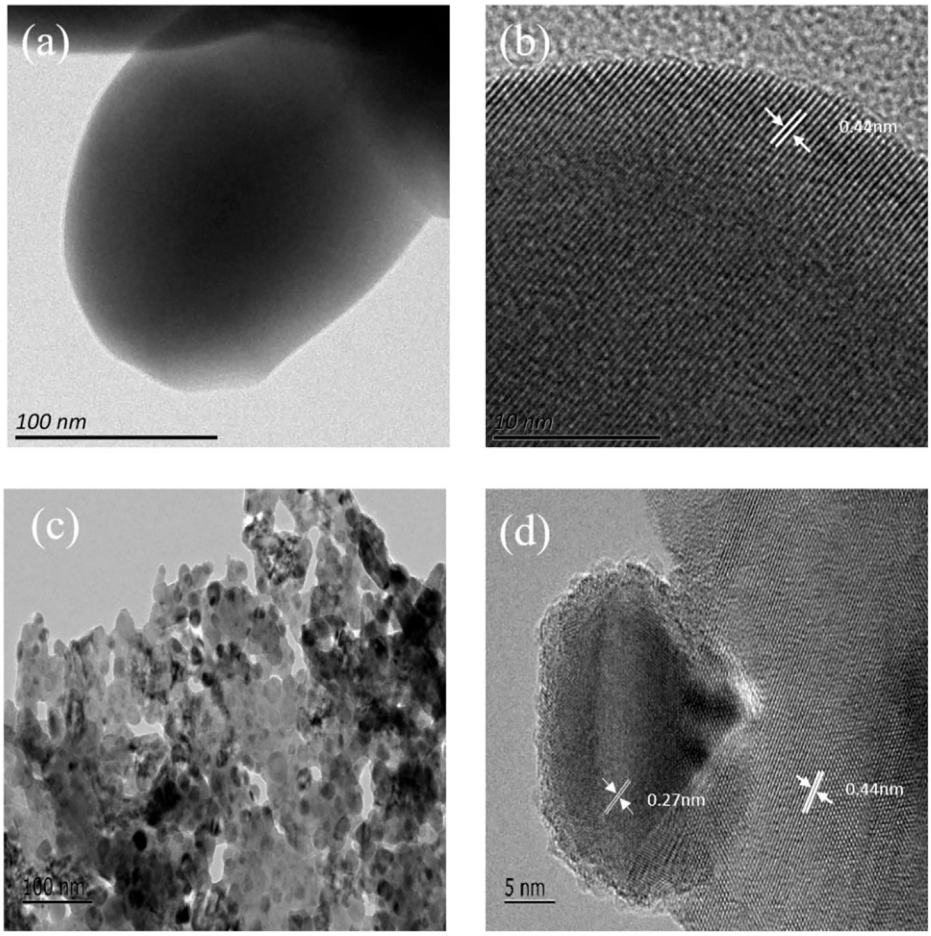

FIGURE 3 | TEM images of **(A,B)** Nb_2O_5 and **(C,D)** 10Ni-10Mn/Nb_2O_5 catalysts.

TABLE 2 | Acidity amount of the catalysts determined by NH_3-TPD.

Sample	Acidity (mmolg^{-1})		
	Total	Medium	Strong
Nb_2O_5	0.811	0	0.811
10Ni-10Mn/Nb_2O_5	1.854	0.823	1.031

observed at the position of 29.9°, which may be ascribed to the reflection of $NiMnO_3$ which need further confirmation by later characterization methods (Vivekanandan et al., 2020). In addition, no obvious diffraction peaks of metallic manganese were observed in the 10Ni-10Mn/Nb_2O_5 catalyst, which was attributed to the low crystallinity or small-size of metallic species. Besides, compared with the crystal diffraction intensity of the Nb_2O_5 support, the peak intensity of 10Ni-10Mn/Nb_2O_5 was relatively weakened, which may be attributed to the decrease of the crystallinity of the carrier as the addition of metal.

XPS analysis was used to confirm the chemical state of the metal elements on the catalyst surface. The spectrum of **Figure 5** recorded the respective valence states of these three elements Ni, Mn, and Nb. It should be clearly seen that there are five binding energy corresponding peaks in the XPS spectrum of Ni (**Figure 5**). Binding energies at 852.1 and 855.1 eV could be

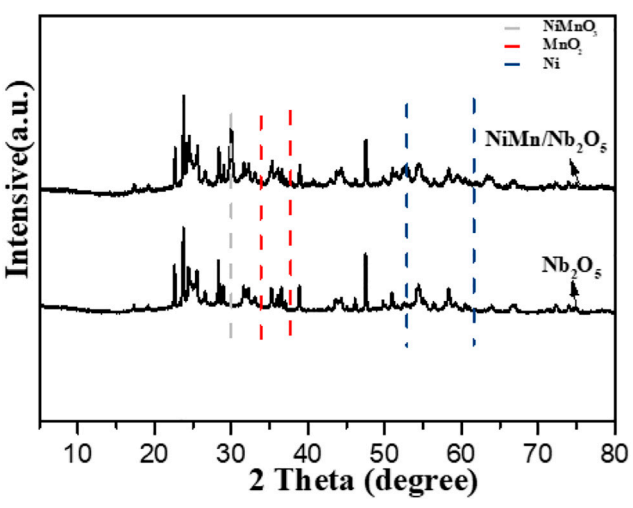

FIGURE 4 | X-ray diffraction pattern of catalysts.

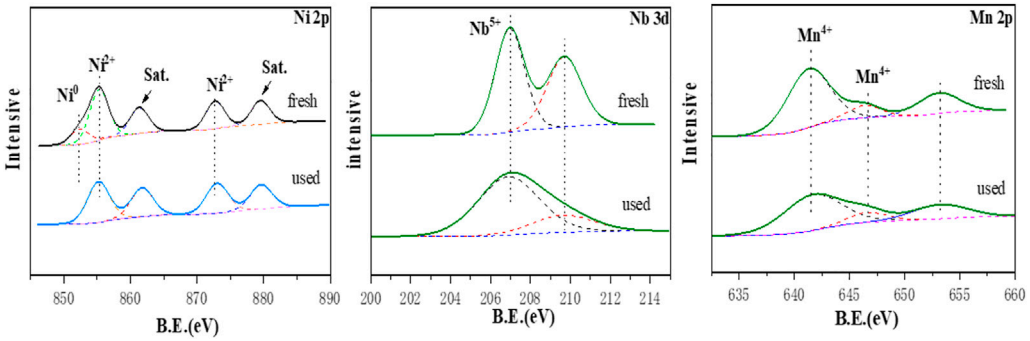

FIGURE 5 | XPS analysis of the reduced and used Ni–Mn/Nb_2O_5 catalysts.

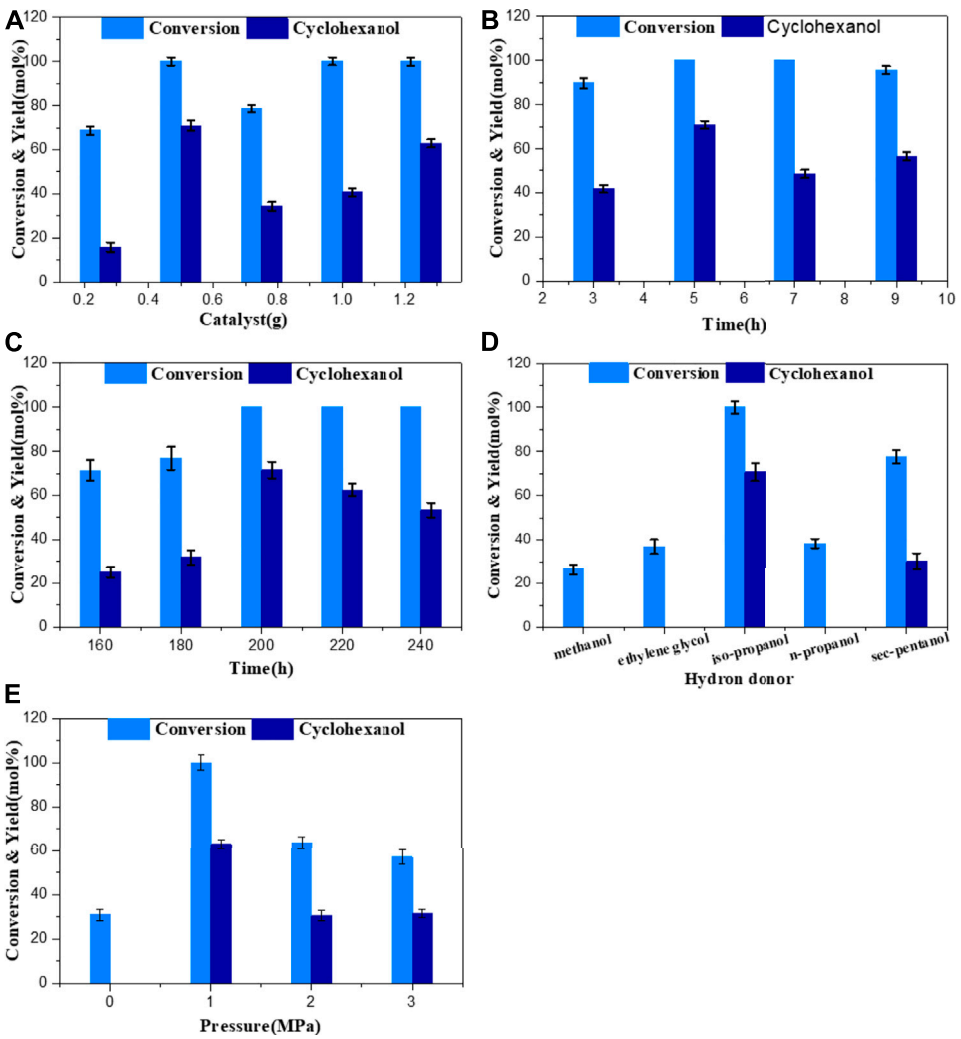

FIGURE 6 | Effect of **(A)** catalyst amount, **(B)** reaction time, **(C)** reaction temperature, **(D)** hydrogen sources, and **(E)** N_2 pressure on GUA conversion and main product yield. Reaction conditions: 1 g GUA and 0.5 g of 10Ni-10Mn/Nb_2O_5.

attributed to the main line of $Ni^0$and Ni^{2+}, suggesting the presence of both metallic Ni and NiO on the surface of Nb_2O_5. The binding energies at 873.1 eV attributed to Ni^{2+}. Simultaneously, two peaks at 861.4 and 879.7 eV corresponded to satellite peaks. And, the two different chemical states of Ni element detected were ascribed to the incomplete reduction of nickel oxide during the reduction process of the tube furnace. However, for the manganese element XPS spectrum, the main peaks at 641.3 and 646.3 eV were corresponding to the signal peaks of MnO_2 and its satellite peaks, and no related binding energy peaks of metallic manganese are observed, suggesting that MnO_2 was the present form of Mn element on the surface of the Nb_2O_5 support. The peaks centered at 206.9 eV, which was attributed to Nb in Nb_2O_5. In addition, no other Nb species appeared in spectrum indicating that the metal phase was only impregnated on the surface of the support and not interacted with the metal during the preparation of the catalyst. By comparing with the fresh catalyst in **Figure 5**, it could be found that there was no Ni^0 peak in the XPS spectrum of the spent catalyst, which indicates that the decrease in activity in the catalyst cycle experiment may be due to the absence of the metal active site Ni^0.

Catalytic Activity on the HDO of Guaiacol

To investigate the effect of catalyst usage on the HDO of guaiacol, the conversion of guaiacol and yield of target products cyclohexanol were studied in detail. The catalyst usage was varied from 0.25 to 1.25 g. **Figure 6A** depicts product evolution as a function of catalyst. The upsurge in the guaiacol conversion was consistent with the increase in catalyst usage from 0.25 to 1.25 g. The research shows that guaiacol was completely converted when the amount of catalyst exceeds 0.5 g and obtained the best cyclohexanol yield (70.8%).

Reaction time had a pronounced effect on the conversion of phenolic compounds and the distribution of products. As shown in **Figure 6B**, phenol conversion gradually increased when the reaction time increased from 3 to 5 h. When the reaction time was long enough (>5 h), guaiacol can be completely converted. But for the selectivity of the product, only the change in the yield of cyclohexanol could be clearly observed. When the reaction time was 5 h, the yield of cyclohexanol was the highest. With the further extension of the reaction time, the yield of cyclohexanol decreased that may be due to two reasons: (1) the product underwent a certain degree of polymerization, (2) the catalyst was covered by the polymer and led to partial deactivation. Therefore, using a moderated time 5 h was a prospect process for producing cyclohexanol from the hydrogenation of guaiacol.

The effect of reaction temperature on phenol conversion and product distribution was investigated. The hydrogenation reaction of guaiacol with 10Ni-10Mn/Nb_2O_5 catalyst was carried out at a range from 160°C to 240°C with the interval temperature of 20°C. As shown in **Figure 6C**, the conversion of guaiacol increased with the temperature increasing when the temperature was lower than 200°C. When the temperature reached 200°C, the complete conversion of guaiacol can be realized. However, further increase in temperature (such as 220°C and 240°C) would decrease the yield of the main product cyclohexanol and the possible reason was that the catalyst was partially deactivated at high temperature, or a relatively high temperature could cause the polymerization of products and could cover on the surface of the catalyst, thereby affecting the activity of the catalyst. Therefore, 200°C was the optimal reaction temperature for the conversion of guaiacol with the 10Ni-10Mn/Nb_2O_5 catalyst.

To examine the effects of different organic solvents on the HDO of guaiacol over 10Ni-10Mn/Nb_2O_5 in the solvent system composed of water and organic solvent, several organic solvents such as methanol (CH_3OH), ethylene glycol ($CH_2OH)_2$, isopropanol (C_3H_7OH), *n*-propanol (C_3H_7OH), and sec-pentanol ($C_5H_{11}OH$) were used for the HDO of guaiacol under the same conditions. The yield of cyclohexanol with the different organic solvents is shown in **Figure 6D**. It was worth noting that the catalytic activity and the product yield of 10Ni-10Mn/Nb_2O_5 for selective HDO of guaiacol varied greatly with a change in the different solvents. As the results shown that the HDO reaction of GUA using primary alcohols (ethylene glycol, methanol, and *n*-propanol) as hydrogen donors showed lower reactivity, the conversion of guaiacol was 37, 26.4, and 38.6%, respectively. And, the product of cyclohexanol was not detected. This was mainly because it was difficult to remove β-hydride from the primary alcohol during the reaction that limits its hydrogen supply performance, which was consistent with many previous reports (Kuwahara et al., 2014; Cai et al., 2017). For secondary alcohols, the yield of cyclohexanol was 70.8% in the reaction with isopropanol as the hydrogen donor, and the reaction with secondary amyl alcohol also provided 30.2 mol % of cyclohexanol yield. The system showed a good effect of *in situ* hydrogen production. Therefore, considering its reactivity and practicality, isopropanol was selected as the hydrogen donor for *in situ* hydrogenation to produce cyclohexanol in our system.

The reaction pressure also has a certain influence on the performance of the catalyst. Considering the influence of different reaction pressures on the HDO selectivity of guaiacol, the nitrogen pressure was optimized on the 10Ni-10Mn/Nb_2O_5 catalyst. **Figure 6E** showed the reaction product distribution and conversion of guaiacol. The conversion of guaiacol from 31 to 100% and cyclohexanol yield from 0 to 63% with the N_2 pressure from 0 to 1. However, higher pressure above 2 MPa decreased the guaiacol conversion and cyclohexanol yields. The phenomenon indicated that excessive pressure (above 2 MPa) had a negative effect on the hydrodeoxygenation of guaiacol. It may be desirable that too much pressure led to deactivation of the catalyst, thereby decreasing catalytic performance.

Catalyst Applicability of Different Phenolic Compounds

In order to investigate the applicability of the catalyst in *in situ* hydrogenation, other lignin-derived phenolic compounds were evaluated under 1 MPa N_2 at 200°C for 5 h. The 10Ni-10Mn/Nb_2O_5 catalyst was used for the *in situ* hydrogenation of m-cresol, phenol, ethyl-guaiacol, and 3-methoxyphenol (the common phenolic compounds of bio-oil) employing aqueous reforming reaction from water and isopropanol to produce hydrogen as a hydrogen donor. It could be seen from **Figure 7** that all phenolic compounds could be selectively converted into cyclohexanol compounds and phenolic compounds under the action of a catalyst, showing good hydrodeoxygenation performance. In the GC-MS images of

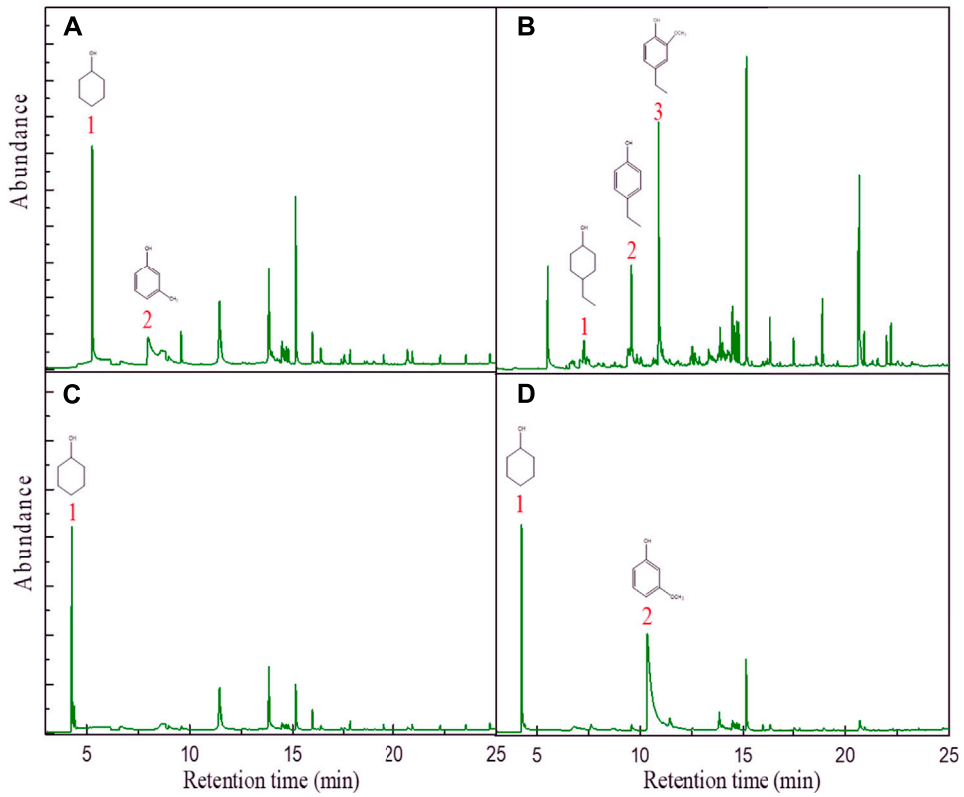

FIGURE 7 | The GC-MS data graph of **(A)** m-cresol, **(B)** ethyl-guaiacol, **(C)** phenol, and **(D)** 3-methoxyphenol. Reaction conditions: 0.5 g of 10Ni-10Mn/Nb_2O_5, 200°C, 5 h, and 1 MPa N_2.

m-cresol and 3-methoxyphenol, only cyclohexanol compounds were observed, and in the other compounds, in addition to cyclohexanol compounds, phenol was also observed. The results showed that, under the action of the catalyst, there was no complete hydrogenation, and the experimental conditions need to be further improved.

Possible Reaction Pathway of Guaiacol over Ni–Mn/Nb_2O_5 Catalyst

We deduced two possible pathways in guaiacol conversion based on the products detected by GC-MS in **Supplementary Figure S2**, with cyclohexanol as the main product. Under the optimal reaction conditions, we observed that the main byproducts of guaiacol hydrodeoxygenation on the catalyst are cyclohexanone and 1-methyl-1,2-cyclohexanediol, and only trace amount of phenol is produced.

As shown in **Supplementary Figure S2**, only trace amount of phenol is detected as phenol can be quickly hydrogenated to cyclohexanol, which was already confirmed. In addition, through the hydrodeoxygenation of phenol, the byproduct cyclohexanone was found. Therefore, we believe that there is a reaction path in which phenol is first hydrogenated to cyclohexanone and then further hydrogenated to cyclohexanol. In comparison with the amount of phenol, a relatively large amount of 1-methyl-1,2-cyclohexanediol is observed. According to reports in the literature (Zhou et al., 2017b) (Song et al., 2020), 1-methyl-1,2-cyclohexanediol can be used as an intermediate of cyclohexanol, so another reaction pathway to produce cyclohexanol is obtained. The proposed reaction pathway of guaiacol is demonstrated in **Figure 8**.

Applicability of the Recycled Catalyst

To examine the reusability of 10Ni-10Mn/Nb_2O_5 in the *in situ* hydrogenation of guaiacol, the stability of the catalyst was important for its practical usage. Therefore, the 10Ni-10Mn/Nb_2O_5 catalyst was subjected to stability testing by recycling the same catalyst for four consecutive cycles for guaiacol HDO reaction. At the end of each cycle, the catalyst was recovered from the reactor by filtration and dried overnight at 60°C. Due to the loss of part of the catalyst in the process of recovering the catalyst, this catalyst loss was compensated by adding a fresh catalyst. The results of stability test are shown in **Figure 9**. The catalyst was reused three times, and the conversion of guaiacol remained at 100%. However, the yield of the main product cyclohexanol gradually decreased, and the yield of cyclohexanol was reduced from 59.2 to 44.5% after repeated use. It may be because in the process of reuse, some metal sites on the catalyst lose their activity in the reaction, which leads to a decrease in the product yield. In addition, a regeneration experiment was carried out on the catalyst. After

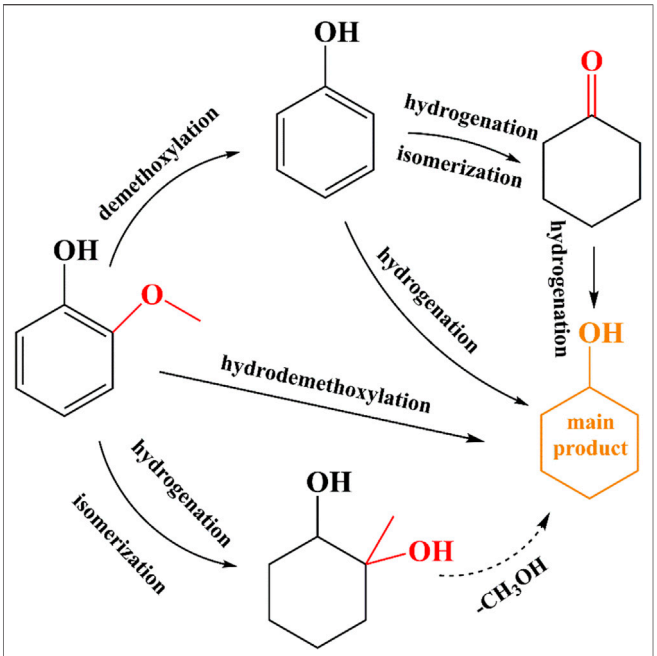

FIGURE 8 | Possible reaction pathway for the conversion of guaiacol over Ni–Mn/Nb_2O_5.

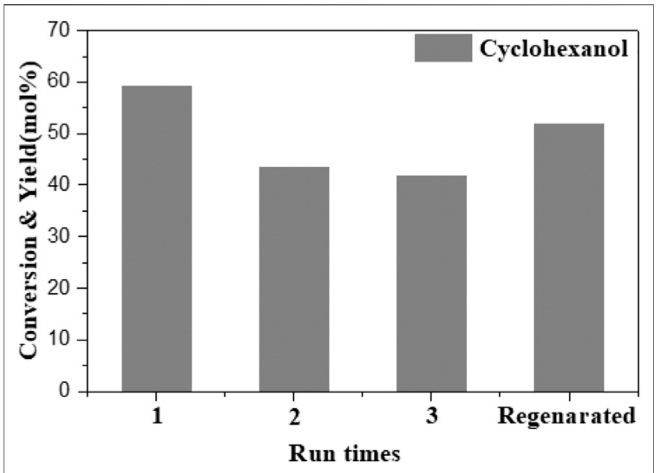

FIGURE 9 | The reusability test of the 10Ni-10Mn/Nb_2O_5 catalyst.

calcination in a muffle furnace at 500°C for 3 h in air and reduction with hydrogen in a tube furnace at 500°C for 3 h, the catalyst activity almost recovered to its original activity. It could be seen from the results that the stability of the catalyst is relatively good.

CONCLUSION

In this work, the *in situ* hydrogenation of guaiacol (a typical model compound of bio-oil), using isopropanol as the hydrogen donor, was conducted to measure the catalytic performance of 10Ni-10Mn/Nb_2O_5. The result showed that guaiacol can be efficiently converted into cyclohexanol under mild conditions (200°C, 1 MPa N_2), and the yield of target product cyclohexanol was up to 71.8%, which suggested the catalyst has remarkable hydrogenation performance. The results of hydrogenation of guaiacol with different hydrogen donors indicated isopropanol as the hydrogen donor had better activity. The catalyst had the characteristics of high metal dispersibility and large pore size from SEM, TEM, and BET, which may be helpful for the *in situ* hydrogen production of the hydrogen supply solvent and the hydrogenation process of phenolic chemicals. In addition, the stability of the catalyst was measured by the cyclic properties of guaiacol, and the yield of the target product cyclohexanol slightly decreases with each cycle. It suggested that 10Ni-10Mn/Nb_2O_5 may be partially deactivated during the reaction which the reason will be further proven. Hydroreforming reaction which avoids the need for molecular hydrogen to carry out hydrogenation reactions has some shortcomings and provides an effective reaction way for catalytic hydrogenation of different phenolic compounds.

DATA AVAILABILITY STATEMENT

The original contributions presented in the study are included in the article/**Supplementary Material**. Further inquiries can be directed to the corresponding authors.

AUTHOR CONTRIBUTIONS

LT contributed to data curation, conceptualized the study, and prepared the original draft. BC investigated and validated the study. RZ was responsible for methodology and provided software. JF visualized and supervised the study. HP reviewed and edited the article.

ACKNOWLEDGMENTS

The authors gratefully acknowledge the financial support provided by the Natural Science Fund for Colleges and Universities in Jiangsu Province (20KJB220010) for this investigation. The authors also thank the Research Grant of Jiangsu Province Biomass Energy and Materials Laboratory (JSBEM201903) for this investigation.

SUPPLEMENTARY MATERIAL

The Supplementary Material for this article can be found online at: https://www.frontiersin.org/articles/10.3389/fenrg.2021.746109/full#supplementary-material

REFERENCES

Bjelić, A., Grilc, M., Huš, M., and Likozar, B. (2019). Hydrogenation and Hydrodeoxygenation of Aromatic Lignin Monomers over Cu/C, Ni/C, Pd/C, Pt/C, Rh/C and Ru/C Catalysts: Mechanisms, Reaction Micro-kinetic Modelling and Quantitative Structure-Activity Relationships. *Chem. Eng. J.* 359, 305–320. doi:10.1016/j.cej.2018.11.107

Cai, B., Zhou, X.-C., Miao, Y.-C., Luo, J.-Y., Pan, H., and Huang, Y.-B. (2017). Enhanced Catalytic Transfer Hydrogenation of Ethyl Levulinate to γ-Valerolactone over a Robust Cu-Ni Bimetallic Catalyst. *ACS Sustain. Chem. Eng.* 5, 1322–1331. doi:10.1021/acssuschemeng.6b01677

Chen, L., Xin, J., Ni, L., Dong, H., Yan, D., Lu, X., et al. (2016). Conversion of Lignin Model Compounds under Mild Conditions in Pseudo-homogeneous Systems. *Green. Chem.* 18, 2341–2352. doi:10.1039/c5gc03121d

Chen, M.-Y., Huang, Y.-B., Pang, H., Liu, X.-X., and Fu, Y. (2015). Hydrodeoxygenation of Lignin-Derived Phenols into Alkanes over Carbon Nanotube Supported Ru Catalysts in Biphasic Systems. *Green. Chem.* 17, 1710–1717. doi:10.1039/c4gc01992j

Feng, J., Yang, Z., Hse, C.-y., Su, Q., Wang, K., Jiang, J., et al. (2017). *In Situ* catalytic Hydrogenation of Model Compounds and Biomass-Derived Phenolic Compounds for Bio-Oil Upgrading. *Renew. Energ.* 105, 140–148. doi:10.1016/j.renene.2016.12.054

Ferentz, M., Landau, M. V., Vidruk, R., and Herskowitz, M. (2015). Fixed-bed Catalytic Wet Peroxide Oxidation of Phenol with Titania and Au/titania Catalysts in Dark. *Catal. Today* 241, 63–72. doi:10.1016/j.cattod.2014.05.013

Funkenbusch, L. T., Mullins, M. E., Salam, M. A., Creaser, D., and Olsson, L. (2019). Catalytic Hydrotreatment of Pyrolysis Oil Phenolic Compounds over Pt/Al2O3 and Pd/C. *Fuel* 243, 441–448. doi:10.1016/j.fuel.2019.01.139

Han, G.-H., Lee, M. W., Park, S., Kim, H. J., Ahn, J.-P., Seo, M.-g., et al. (2019). Revealing the Factors Determining the Selectivity of Guaiacol HDO Reaction Pathways Using ZrP-Supported Co and Ni Catalysts. *J. Catal.* 377, 343–357. doi:10.1016/j.jcat.2019.07.034

He, Z., Hu, M., and Wang, X. (2018). Highly Effective Hydrodeoxygenation of Guaiacol on Pt/TiO2: Promoter Effects. *Catal. Today* 302, 136–145. doi:10.1016/j.cattod.2017.02.034

Jin, S., Guan, W., Tsang, C.-W., Yan, D. Y. S., Chan, C.-Y., and Liang, C. (2017). Enhanced Hydroconversion of Lignin-Derived Oxygen-Containing Compounds over Bulk Nickel Catalysts Though Nb2O5 Modification. *Catal. Lett.* 147, 2215–2224. doi:10.1007/s10562-017-2085-6

Kon, K., Onodera, W., Takakusagi, S., and Shimizu, K.-i. (2014). Hydrodeoxygenation of Fatty Acids and Triglycerides by Pt-Loaded Nb2O5 Catalysts. *Catal. Sci. Technol.* 4, 3705–3712. doi:10.1039/c4cy00757c

Kuwahara, Y., Kaburagi, W., and Fujitani, T. (2014). Catalytic Transfer Hydrogenation of Levulinate Esters to γ-valerolactone over Supported Ruthenium Hydroxide Catalysts. *RSC Adv.* 4, 45848–45855. doi:10.1039/c4ra08074b

Li, W., Wang, H., Wu, X., Betancourt, L. E., Tu, C., Liao, M., et al. (2020). Ni/hierarchical ZSM-5 Zeolites as Promising Systems for Phenolic Bio-Oil Upgrading: Guaiacol Hydrodeoxygenation. *Fuel* 274, 117859. doi:10.1016/j.fuel.2020.117859

Li, X., Gunawan, R., Wang, Y., Chaiwat, W., Hu, X., Gholizadeh, M., et al. (2014). Upgrading of Bio-Oil into Advanced Biofuels and Chemicals. Part III. Changes in Aromatic Structure and Coke Forming Propensity during the Catalytic Hydrotreatment of a Fast Pyrolysis Bio-Oil with Pd/C Catalyst. *Fuel* 116, 642–649. doi:10.1016/j.fuel.2013.08.046

Li, Y., Yang, X., Zhu, L., Zhang, H., and Chen, B. (2015). Hydrodeoxygenation of Phenol as a Bio-Oil Model Compound over Intimate Contact noble Metal-Ni2P/SiO2 Catalysts. *RSC Adv.* 5, 80388–80396. doi:10.1039/c5ra11203f

Liu, K., Yan, P., Jiang, H., Xia, Z., Xu, Z., Bai, S., et al. (2019). Silver Initiated Hydrogen Spillover on Anatase TiO2 Creates Active Sites for Selective Hydrodeoxygenation of Guaiacol. *J. Catal.* 369, 396–404. doi:10.1016/j.jcat.2018.11.033

Lu, M., Sun, Y., Zhang, P., Zhu, J., Li, M., Shan, Y., et al. (2019). Hydrodeoxygenation of Guaiacol Catalyzed by High-Loading Ni Catalysts Supported on SiO2-TiO2 Binary Oxides. *Ind. Eng. Chem. Res.* 58, 1513–1524. doi:10.1021/acs.iecr.8b04517

Ma, D., Lu, S., Liu, X., Guo, Y., and Wang, Y. (2019). Depolymerization and Hydrodeoxygenation of Lignin to Aromatic Hydrocarbons with a Ru Catalyst on a Variety of Nb-Based Supports. *Chin. J. Catal.* 40, 609–617. doi:10.1016/s1872-2067(19)63317-6

Montañez Valencia, M. K., Padró, C. L., and Sad, M. E. (2020). Gas Phase Acylation of Guaiacol with Acetic Acid on Acid Catalysts. *Appl. Catal. B Environ.* 278, 119317. doi:10.1016/j.apcatb.2020.119317

Mortensen, P. M., Grunwaldt, J.-D., Jensen, P. A., and Jensen, A. D. (2016). Influence on Nickel Particle Size on the Hydrodeoxygenation of Phenol over Ni/SiO 2. *Catal. Today* 259, 277–284. doi:10.1016/j.cattod.2015.08.022

Mushtaq, F., Abdullah, T. A. T., Mat, R., and Ani, F. N. (2015). Optimization and Characterization of Bio-Oil Produced by Microwave Assisted Pyrolysis of Oil palm Shell Waste Biomass with Microwave Absorber. *Bioresour. Techn.* 190, 442–450. doi:10.1016/j.biortech.2015.02.055

Newman, C., Zhou, X., Goundie, B., Ghampson, I. T., Pollock, R. A., Ross, Z., et al. (2014). Effects of Support Identity and Metal Dispersion in Supported Ruthenium Hydrodeoxygenation Catalysts. *Appl. Catal. A: Gen.* 477, 64–74. doi:10.1016/j.apcata.2014.02.030

Ohta, H., Feng, B., Kobayashi, H., Hara, K., and Fukuoka, A. (2014). Selective Hydrodeoxygenation of Lignin-Related 4-propylphenol into N-Propylbenzene in Water by Pt-Re/ZrO2 Catalysts. *Catal. Today* 234, 139–144. doi:10.1016/j.cattod.2014.01.022

Qin, L., Yi, H., Zeng, G., Lai, C., Huang, D., Xu, P., et al. (2019). Hierarchical Porous Carbon Material Restricted Au Catalyst for Highly Catalytic Reduction of Nitroaromatics. *J. Hazard. Mater.* 380, 120864. doi:10.1016/j.jhazmat.2019.120864

Qiu, S., Xu, Y., Weng, Y., Ma, L., and Wang, T. (2016). Efficient Hydrogenolysis of Guaiacol over Highly Dispersed Ni/MCM-41 Catalyst Combined with HZSM-5. *Catalysts* 6, 9–13. doi:10.3390/catal6090134

Ragauskas, A. J., Beckham, G. T., Biddy, M. J., Chandra, R., Chen, F., Davis, M. F., et al. (2014). Lignin Valorization: Improving Lignin Processing in the Biorefinery. *Science* 344, 1246843. doi:10.1126/science.1246843

Rahzani, B., Saidi, M., Rahimpour, H. R., Gates, B. C., and Rahimpour, M. R. (2017). Experimental Investigation of Upgrading of Lignin-Derived Bio-Oil Component Anisole Catalyzed by Carbon Nanotube-Supported Molybdenum. *RSC Adv.* 7, 10545–10556. doi:10.1039/c6ra26121c

Reddy Kannapu, H. P., Mullen, C. A., Elkasabi, Y., and Boateng, A. A. (2015). Catalytic Transfer Hydrogenation for Stabilization of Bio-Oil Oxygenates: Reduction of P-Cresol and Furfural over Bimetallic Ni-Cu Catalysts Using Isopropanol. *Fuel Process. Techn.* 137, 220–228. doi:10.1016/j.fuproc.2015.04.023

Resende, K. A., Braga, A. H., Noronha, F. B., and Hori, C. E. (2019). Hydrodeoxygenation of Phenol over Ni/Ce1-xNbxO2 Catalysts. *Appl. Catal. B Environ.* 245, 100–113. doi:10.1016/j.apcatb.2018.12.040

Saidi, M., Samimi, F., Karimipourfard, D., Nimmanwudipong, T., Gates, B. C., and Rahimpour, M. R. (2014). Upgrading of Lignin-Derived Bio-Oils by Catalytic Hydrodeoxygenation. *Energy Environ. Sci.* 7, 103–129. doi:10.1039/c3ee43081b

Shafaghat, H., Tsang, Y. F., Jeon, J.-K., Kim, J. M., Kim, Y., Kim, S., et al. (2020). *In-situ* Hydrogenation of Bio-Oil/bio-Oil Phenolic Compounds with Secondary Alcohols over a Synthesized Mesoporous Ni/CeO2 Catalyst. *Chem. Eng. J.* 382, 122912. doi:10.1016/j.cej.2019.122912

Shu, R., Lin, B., Zhang, J., Wang, C., Yang, Z., and Chen, Y. (2019). Efficient Catalytic Hydrodeoxygenation of Phenolic Compounds and Bio-Oil over Highly Dispersed Ru/TiO2. *Fuel Process. Techn.* 184, 12–18. doi:10.1016/j.fuproc.2018.11.004

Song, W., He, Y., Lai, S., Lai, W., Yi, X., Yang, W., et al. (2020). Selective Hydrodeoxygenation of Lignin Phenols to Alcohols in the Aqueous Phase over a Hierarchical Nb2O5-Supported Ni Catalyst. *Green. Chem.* 22, 1662–1670. doi:10.1039/c9gc03842f

Vivekanandan, A. K., Subash, V., Chen, S.-m., and Chen, S.-H. (2020). Sonochemical Synthesis of Nickel-Manganous Oxide Nanocrumbs Decorated Partially Reduced Graphene Oxide for Efficient Electrochemical Reduction of Metronidazole. *Ultrason. Sonochem.* 68, 105176. doi:10.1016/j.ultsonch.2020.105176

Wang, H., Zhao, F., Fujita, S.-i., and Arai, M. (2008). Hydrogenation of Phenol in scCO2 over Carbon Nanofiber Supported Rh Catalyst. *Catal. Commun.* 9, 362–368. doi:10.1016/j.catcom.2007.07.002

Xu, Y., Li, Y., Wang, C., Wang, C., Ma, L., Wang, T., et al. (2017). *In-situ* Hydrogenation of Model Compounds and Raw Bio-Oil over Ni/CMK-3

Catalyst. *Fuel Process. Techn.* 161, 226–231. doi:10.1016/j.fuproc.2016.08.018

Xu, Y., Long, J., Liu, Q., Li, Y., Wang, C., Zhang, Q., et al. (2015). *In Situ* hydrogenation of Model Compounds and Raw Bio-Oil over Raney Ni Catalyst. *Energ. Convers. Manag.* 89, 188–196. doi:10.1016/j.enconman.2014.09.017

Yang, F., Libretto, N. J., Komarneni, M. R., Zhou, W., Miller, J. T., Zhu, X., et al. (2019). Enhancement of M-Cresol Hydrodeoxygenation Selectivity on Ni Catalysts by Surface Decoration of MoOx Species. *ACS Catal.* 9, 7791–7800. doi:10.1021/acscatal.9b01285

Zhang, X., Tang, W., Zhang, Q., Wang, T., and Ma, L. (2018). Hydrodeoxygenation of Lignin-Derived Phenoic Compounds to Hydrocarbon Fuel over Supported Ni-Based Catalysts. *Appl. Energ.* 227, 73–79. doi:10.1016/j.apenergy.2017.08.078

Zhao, H. Y., Li, D., Bui, P., and Oyama, S. T. (2011). Hydrodeoxygenation of Guaiacol as Model Compound for Pyrolysis Oil on Transition Metal Phosphide Hydroprocessing Catalysts. *Appl. Catal. A: Gen.* 391, 305–310. doi:10.1016/j.apcata.2010.07.039

Zhou, M., Ye, J., Liu, P., Xu, J., and Jiang, J. (2017). Water-Assisted Selective Hydrodeoxygenation of Guaiacol to Cyclohexanol over Supported Ni and Co Bimetallic Catalysts. *ACS Sustain. Chem. Eng.* 5, 8824–8835. doi:10.1021/acssuschemeng.7b01615

Zhou, M., Ye, J., Liu, P., Xu, J., and Jiang, J. (2017). Water-Assisted Selective Hydrodeoxygenation of Guaiacol to Cyclohexanol over Supported Ni and Co Bimetallic Catalysts. *ACS Sustain. Chem. Eng.* 5, 8824–8835. doi:10.1021/acssuschemeng.7b01615

Zhu, X., Lobban, L. L., Mallinson, R. G., and Resasco, D. E. (2011). Bifunctional Transalkylation and Hydrodeoxygenation of Anisole over a Pt/HBeta Catalyst. *J. Catal.* 281, 21–29. doi:10.1016/j.jcat.2011.03.030

Conflict of Interest: The authors declare that the research was conducted in the absence of any commercial or financial relationships that could be construed as a potential conflict of interest.

Publisher's Note: All claims expressed in this article are solely those of the authors and do not necessarily represent those of their affiliated organizations, or those of the publisher, the editors, and the reviewers. Any product that may be evaluated in this article, or claim that may be made by its manufacturer, is not guaranteed or endorsed by the publisher.